Heteroclinic Bifurcations and Invariant Manifolds in Rocking Block Dynamics

B. Bruhn and B. P. Koch

Fachbereich Physik, Ernst-Moritz-Arndt-Universität, Greifswald, Germany

Z. Naturforsch. **46a**, 481–490 (1991); received February 13, 1991

A simple model of rigid block motion under the influence of external perturbations is discussed. For periodic forcings we prove the existence of Smale horseshoe chaos in the dynamics. For slender blocks a heteroclinic bifurcation condition is calculated exactly, i.e. without using perturbation methods. That means that our results are valid for arbitrary excitation amplitudes. Furthermore, analytical formulas for the first pieces of the stable and unstable manifolds are derived not only for periodically but also for transiently driven systems. In the case of small excitation and damping the Melnikov method is used to treat the full nonlinear problem.

Key words: Earthquake dynamics, Heteroclinic bifurcations, Melnikov method, Chaos.

1. Introduction

Rocking response of a rigid structure to an external time dependent perturbation shows a very sensitive dependence upon the system parameters and the initial conditions. Recently a series of papers were published giving numerical evidence and experimental indications of such complicated behaviour [1–5]. The rocking block dynamics is a particularly important topic because the effect of an earthquake on man-made structures for instance on towers, nuclear reactors, residential buildings etc. can be studied. A block may overturn depending on the geometrical form of the block, the initial conditions and the parameters (frequency, amplitude) of the external perturbation. The precarious initial conditions are determined by the basin boundaries of a certain set of stable fixed points. It is well known [6] that the basin boundaries can have a very complicated fractal structure. Therefore one can understand the observation made in realistic experiments that often some blocks remain standing while other identical ones topple [4]. It should be noted that a real earthquake has always a finite duration and can only be approximately described by a periodic perturbation. Therefore transiently forced dynamics represents a more realistic model. Similar dynamical systems with an exponentially decaying forcing can be found in [7, 8], where the analysis shows that such type of forcing produces truncated-fractal basin boundaries. Moreover, it is impossible to extract a Smale horseshoe map [9] which is essentially based on the periodicity in time of the perturbation. However, one can expect a very complicated transient motion of the block.

In this paper we study the standard model (see Fig. 1) of a rocking block as given in the engineering literature. The block is assumed to be rigid and uniform so that the gravity acts in the geometric centre.

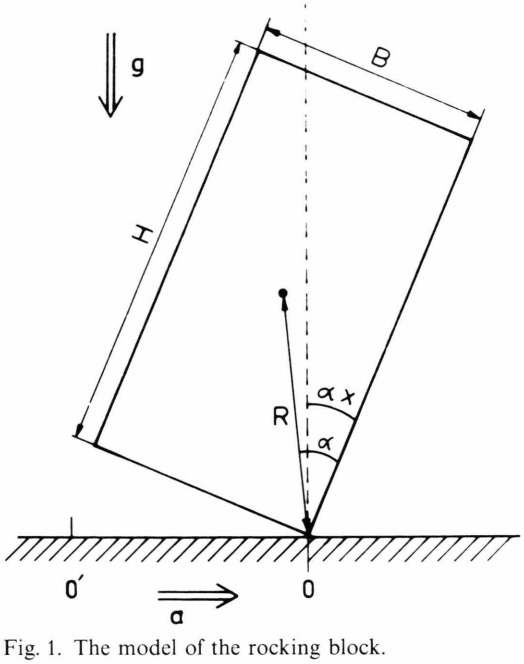

Fig. 1. The model of the rocking block.

Reprint requests to B. Bruhn and B. P. Koch, Fachbereich Physik, Universität Greifswald, Domstraße 10a, O-2200 Greifswald.

0932-0784 / 91 / 0600-0481 $ 01.30/0. – Please order a reprint rather than making your own copy.

Sliding and bouncing of the block are not considered, and the action of an earthquake is given by a horizontal component of the acceleration $a(t)$. Therefore the motion of the block can be described by a single dynamical variable $x(t)$ as a rotation around O and O′ in Fig. 1, respectively. With a periodic forcing one obtains the following equation of motion [4]:

$$\alpha\ddot{x} \pm \sin[\alpha(1 \mp x)] = -\alpha\beta\cos[\alpha(1 \mp x)]\cos(\omega t), \quad (1.1)$$

where the upper (lower) sign is valid for rocking about O, i.e. for $x > 0$ (for rocking about O′, i.e. $x < 0$). β is the dimensionless amplitude of the external perturbation, and the block angle α is defined by $\tan(\alpha) \equiv B/H$. The dot means differentiation with respect to the dimensionless time variable t,

$$t \equiv \tau(3g/4R)^{1/2}.$$

τ is the time in seconds and g is the acceleration due to gravity. ω is a dimensionless frequency normalized in units of $(3g/4R)^{-1/2}$. A particularity of the model is a discontinuous damping at impact. The energy loss of the block at $x = 0$ is represented by a coefficient of restitution r with

$$\dot{x}(t_A) = r\dot{x}(t_B), \quad (1.2)$$

where $0 \leq r \leq 1$. t_A (t_B) is the time just after (before) the impact. Equation (1.1), completed by the impact rule (1.2), describes a nonlinear dynamical system with a piecewise smooth right-hand side, which becomes topologically equivalent to a pendulum in the case $r = 1$, $\beta = 0$.

The paper is divided into two parts. In Sect. 2 we consider the motion of a slender block ($\alpha \ll 1$). Then (1.1) becomes a piecewise linear equation. The piecewise linear nature allows an exact calculation of the conditions for the onset of subharmonic and heteroclinic bifurcations. Also pieces of the manifolds of hyperbolic fixed points of the Poincaré map can be expressed by analytical formulas. Furthermore, two different types of transiently forced systems (exponentially decaying forcing and single pulse forcing) are considered for the motion of a slender block. In Sect. 3 the Melnikov method is applied to the nonlinear problem (1.1) and (1.2) in the case of small excitation and a coefficient of restitution near 1. We summarize briefly in Section 4.

2. Heteroclinic Bifurcations for Slender Blocks

In the case of slender blocks ($\alpha \ll 1$) the governing equation can be simplified to give the piecewise linear system

$$\dot{x} = y, \quad \dot{y} = x \mp 1 - \beta\cos(\omega t), \quad (2.1)$$

which is completed by the impact rule (1.2). Also in this equation the upper (lower) sign is valid for $x > 0$ ($x < 0$).

The advantage of using piecewise linear systems like (2.1) is given by the fact that one can exactly solve (2.1) in the right and in the left half plane, respectively. To continue the solution into the other half plane, the impact rule (1.2) has to be taken into account. That means solution curves have to be fitted together. At $x = 0$ phase-plane orbits show a discontinuity for $r \neq 1$.

Piecewise linear systems with periodic forcing were investigated in numerous papers. In contrast to other periodically excited systems like the forced pendulum or the Duffing oscillator some bifurcation sequences can be located in parameter space without using perturbation methods. Such systems were investigated by Shaw and Holmes [10–12], Hindmarsh and Jeffries [13] and Kiemel and Holmes [14] with analytical and numerical methods. Chow and Shaw [15] have investigated a system similar to (2.1) but with continuous damping instead of impact losses. Purely numerical methods are used in the papers of Shulman [16], Thompson and Ghaffari [17] and Isomäki et al. [18, 19] to discuss bifurcations to periodic and chaotic motions.

The piecewise linear system (2.1) with the impact rule (1.2) was investigated by Hogan [4] and by Tso and Wong [5]. Hogan has calculated sequences of saddle-node bifurcations for symmetric orbits of period nT (T external period, $n = 1, 3, 5, \ldots$) and also the following symmetry breaking bifurcations.

The mentioned symmetric orbits are invariant with respect to the transformation $(x, y) \to (-x, -y)$ and are characterized by two impacts per period. The saddle-node bifurcations appear for an excitation.

$$\beta = \frac{(1+\omega^2)(1-r)(\cosh(n\pi/\omega)-1)}{\sqrt{\omega^2(1-r)^2\sinh^2(n\pi/\omega)+(1+r)^2(\cosh(n\pi/\omega)+1)^2}}. \quad (2.2)$$

A similar formula can be calculated for the symmetry breaking transformation which destabilizes the stable orbit of period nT, but the complete formula is not given by Hogan.

Equation (2.1) has two unique periodic solutions in the right and left half plane, respectively. These orbits are given by

$$\tilde{x}_\pm = \pm 1 + \gamma\cos(\omega t), \quad \tilde{y}_\pm = -\gamma\omega\sin(\omega t), \quad (2.3)$$

where $\gamma = \beta/(1+\omega^2)$. Here the plus (minus) sign is valid in the right (left) half plane. These orbits are of saddle type and reduce to the saddle point at $(x, y) = (\pm 1, 0)$ if $\beta = 0$.

The stable and unstable manifolds of the hyperbolic orbits (2.3) may intersect and therefore give rise to the complicated horseshoe dynamics [9]. The stable and unstable manifolds are defined as those sets of points which are respectively forward and backward asymptotic to the hyperbolic solutions (2.3). Since the system (2.1) is piecewise smooth, but discontinuous (for $r \neq 1$), these sets are themselves disconnected. Nevertheless, these sets are referred to as manifolds.

The formation of crossings of manifolds also plays an important role in the birth of long period motions [20, 21]. Intersections of the manifolds of (2.3) may be calculated using the general solution of (2.1) which is given by

$$\begin{aligned} x_\pm(t) &= c_1^\pm e^t + c_2^\pm e^{-t} + \gamma \cos(\omega t) \pm 1, \\ y_\pm(t) &= c_1^\pm e^t - c_2^\pm e^{-t} - \gamma\omega \sin(\omega t) \end{aligned} \tag{2.4}$$

with the same sign convention as in (2.3). The constants $c_1^\pm$, $c_2^\pm$ are determined by the initial conditions

$$x_\pm(t_0) = x_0^\pm, \quad y_\pm(t_0) = y_0^\pm .$$

From this we have

$$\begin{aligned} c_1^\pm &= \tfrac{1}{2}(x_0^\pm + y_0^\pm - \gamma \cos(\omega t_0) \\ &\quad + \gamma\omega \sin(\omega t_0) \mp 1) \exp(-t_0), \\ c_2^\pm &= \tfrac{1}{2}(x_0^\pm - y_0^\pm - \gamma \cos(\omega t_0) \\ &\quad - \gamma\omega \sin(\omega t_0) \mp 1) \exp(t_0). \end{aligned} \tag{2.5}$$

With (2.4) and (2.5) the manifolds of (2.3) can be calculated. For the right periodic solutions one obtains, by setting $c_1^+ = 0$, for the first piece of the stable manifold

$$y_+^s = -x_+^s + 1 + \gamma \cos(\omega t_0) - \gamma\omega \sin(\omega t_0), \; x_+^s > 0 \tag{2.6}$$

and for the unstable manifold ($c_2^+ = 0$)

$$y_+^u = x_+^u - 1 - \gamma \cos(\omega t_0) - \gamma\omega \sin(\omega t_0), \quad x_+^u < 0. \tag{2.7}$$

These equations may be interpreted as pieces of the manifolds on the cross section

$$\Sigma(t_0) = \{(x, y, t) \mid t = t_0 \bmod (2\pi/\omega)\}. \tag{2.8}$$

By setting $c_1^- = 0$ and $c_2^- = 0$, respectively, one obtains for the stable manifold of the left periodic solution

$$y_-^s = -x_-^s - 1 + \gamma \cos(\omega t_0) - \gamma\omega \sin(\omega t_0), \; x_-^s < 0 \tag{2.9}$$

and for the unstable manifold

$$y_-^u = x_-^u + 1 - \gamma \cos(\omega t_0) - \gamma\omega \sin(\omega t_0), \; x_-^u < 0. \tag{2.10}$$

At $x = 0$ the manifolds show a discontinuity characterized by the coefficient of restitution r ($r < 1$). For $r = 1$ at $x = 0$ the manifolds are continuous but not smooth. Using the solution (2.4) together with (2.5) it is a simple task to continue the manifolds into the other half plane until they once more reach $x = 0$. In this manner one can pursue the manifolds as long as desired. That means we obtain analytical formulas for pieces of manifolds, e.g. the expression for the continuation of the stable manifold (2.6) into the left half plane on the cross section $\Sigma(0)$ is given in a parametric representation by

$$\begin{aligned} x_+^s + y_+^s &= [1 + r + (1-r)\gamma \cos\omega\tau \\ &\quad - (1-r)\gamma\omega \sin\omega\tau] e^{-\tau}/r + \gamma - 1, \\ x_+^s - y_+^s &= [r - 1 - (1+r)\gamma \cos\omega\tau \\ &\quad + (1-r)\gamma\omega \sin\omega\tau] e^{\tau}/r + \gamma - 1, \end{aligned} \tag{2.11}$$

where $0 < \tau < 2\pi/\omega$, $x_+^s < 0$.

Similarly the expressions for the continuation of the unstable manifold (2.10) into the right half plane read as follows:

$$\begin{aligned} x_-^u + y_-^u &= -[1 - r + (1+r)\gamma \cos\omega\tau \\ &\quad + (1-r)\gamma\omega \sin\omega\tau] e^{\tau} + \gamma + 1, \\ x_-^u - y_-^u &= -[1 + r + \gamma(1-r) \\ &\quad \cdot (\cos\omega t - \omega \sin\omega\tau)] e^{-\tau} + \gamma + 1, \end{aligned} \tag{2.12}$$

where $0 < \tau < 2\pi/\omega$, $x_-^u > 0$.

With the help of (2.6)–(2.12) the distance between the stable and unstable manifolds can be calculated. The simplest way to do this is to take a fixed x-value (e.g. $x = 0$) and then to calculate the difference of the y coordinates of the manifolds. Using (2.6) and (2.10) and taking the discontinuity into account, i.e. approaching $x = 0$ e.g. from the right side, we obtain

$$\begin{aligned} \Delta(t_0) &\equiv y_+^s(t_0) - y_-^u(t_0) \\ &= 1 + \gamma \cos\omega t_0 - \gamma\omega \sin\omega t_0 \\ &\quad - r[1 - \gamma \cos\omega t_0 - \gamma\omega \sin\omega t_0] \\ &= 1 - r + \gamma(1+r) \cos\omega t_0 - \gamma\omega(1-r) \sin\omega t_0 . \end{aligned} \tag{2.13}$$

The defined function $\Delta(t_0)$ resembles the usual Melnikov function [9]. But unlike the Melnikov function, which is a first order distance measure with respect to a small perturbation parameter, $\Delta(t_0)$ gives the exact distance between the regarded manifolds and is valid

for arbitrary excitation and damping. Because $1-r \geq 0$ we have to determine the minimum of $\Delta(t_0)$ to obtain the condition for heteroclinic bifurcations, i.e. we seek the smallest value of γ (or β) for which (with fixed values of r and ω) $\Delta(t_0)$ has zeros. After some algebra we obtain

$$\beta = \gamma(1+\omega^2) = \frac{(1+\omega^2)(1-r)}{\sqrt{(1+r)^2+\omega^2(1-r)^2}}. \qquad (2.14)$$

For parameter values β, ω, r which fulfill (2.14) there are quadratic heteroclinic tangencies. For higher values of β (and the same ω, r) the manifolds intersect transversely giving rise to horseshoe dynamics [9]. Holmes [22] and Bertozzi [23] have discussed generalizations of the horseshoe map. The corresponding heteroclinic theorem, which is applicable in our case, is formulated and proved in [23]. Also the results of Gavrilov and Shilnikov [20, 21] can be extended to our case. That means, the saddle-node bifurcations with increasing period accumulate in the parameter space on the heteroclinic bifurcations (2.14). This can be shown explicitly by calculating the limit in (2.2) for $n \to \infty$. The same applies to the mentioned symmetry breaking bifurcations and the subsequent period doubling bifurcations.

According to (2.14) Fig. 2 shows the bifurcation value of β in dependence of ω for different coefficients r. The higher the excitation frequency ω, the more strongly the system has to be forced to get horseshoe dynamics. If there is no energy loss due to impacts (i.e. $r=1$) any arbitrarily small β produces transverse heteroclinic crossings as can be seen in (2.14). The course of the first two pieces of the stable and unstable manifolds of the Poincaré map on the cross section $\Sigma(0)$, defined by (2.6), (2.7), and (2.9)–(2.12), is shown in Figs. 3–5 for different parameter sets. The predicted crossings are clearly visible.

The boundary in phase space which separates simple rocking from tumbling is given by the stable manifold of the hyperbolic orbits (2.3). In the case of transverse heteroclinic crossings this boundary is fractal.

Real earthquakes are characterized by transient forcings. To discuss the effects of such excitations on the tumbling behaviour of blocks two examples are treated. First, we discuss the influence of a single impulse, which is described by a sech function, on the stability of the moving block. The treated equation is

$$\dot{x} = y, \quad \dot{y} = x \mp 1 - \beta \operatorname{sech}(t) \qquad (2.15)$$

with the impact rule (1.2) and the usual sign convention (see e.g. (2.1)). Since the forcing shrinks exponentially to zero, this system shows no chaotic behaviour. The attractors are the asymptotically stable fixed points of the unforced and damped block system. A similar system is treated by Taki [24].

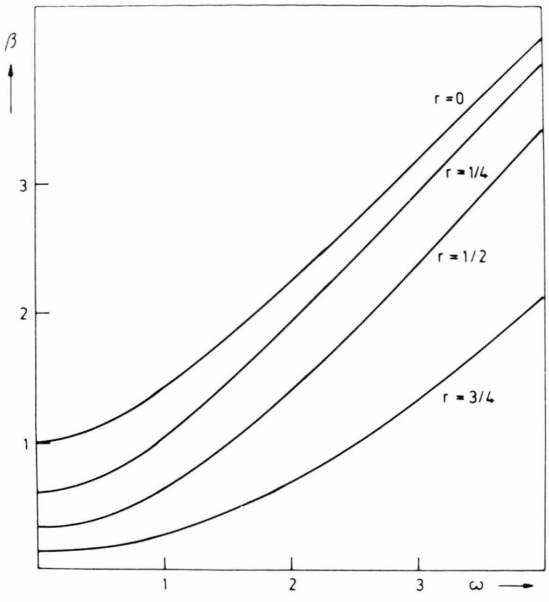

Fig. 2. Heteroclinic bifurcation function (2.14).

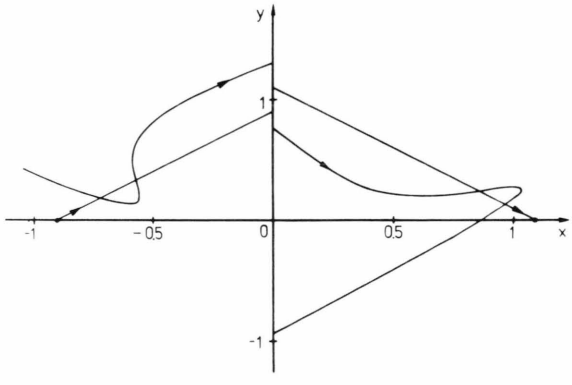

Fig. 3. Pieces of the stable and unstable manifolds of the periodic solutions (2.3) on the cross section $\Sigma(0)$ according to (2.6), (2.7), (2.9)–(2.12). Parameter set: $\beta=0.5$, $\omega=2$, $r=0.85$.

The solution of (2.15) in the two half planes may be represented as

$$x_{\pm}(t) = c_1^{\pm} e^{t} + c_2^{\pm} e^{-t} \pm 1 - \beta[t \cdot \sinh(t) - \cosh(t) \ln(2\cosh(t))],$$
$$y_{\pm}(t) = c_1^{\pm} e^{t} - c_2^{\pm} e^{-t} - \beta[t \cdot \cosh(t) - \sinh(t) \ln(2\cosh(t))], \qquad (2.16)$$

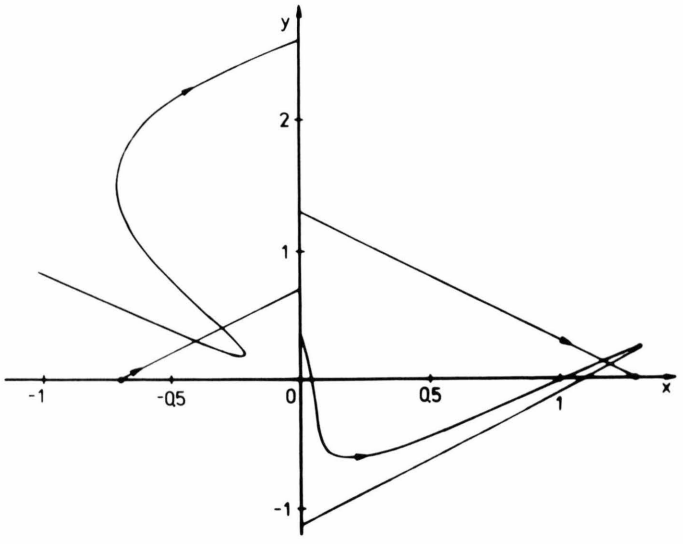

Fig. 4. Pieces of the stable and unstable manifolds of the periodic solutions (2.3) on the cross section $\Sigma(0)$ according to (2.6), (2.7), (2.9)–(2.12). Parameter set: $\beta=1.5$, $\omega=2$, $r=0.5$.

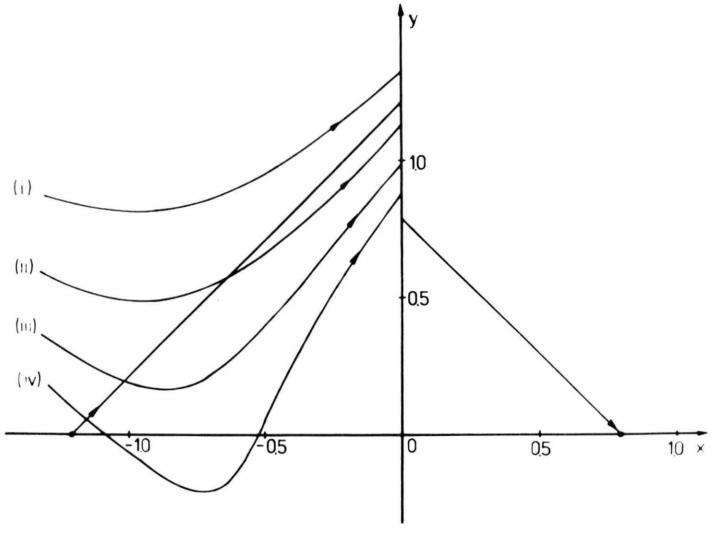

Fig. 6. Pieces of the stable manifold of the right nonperiodic solution (2.17) on the cross section $\Sigma(0)$ according to (2.18), (2.19) for different values of r. Parameter set: $\beta=-0.3$, (i) $r=0.6$, (ii) $r=0.7$, (iii) $r=0.8$, (iv) $r=0.9$.

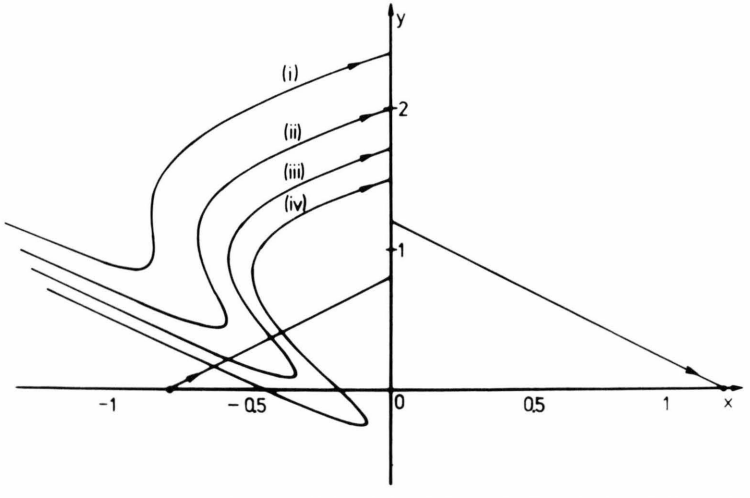

Fig. 5. Pieces of the stable manifold of the right periodic solution (2.3) on the cross section $\Sigma(0)$ according to (2.6), (2.11) for different values of r. Parameter set: $\beta=1$, $\omega=2$, (i) $r=0.5$, (ii) $r=0.6$, (iii) $r=0.7$, (iv) $r=0.8$.

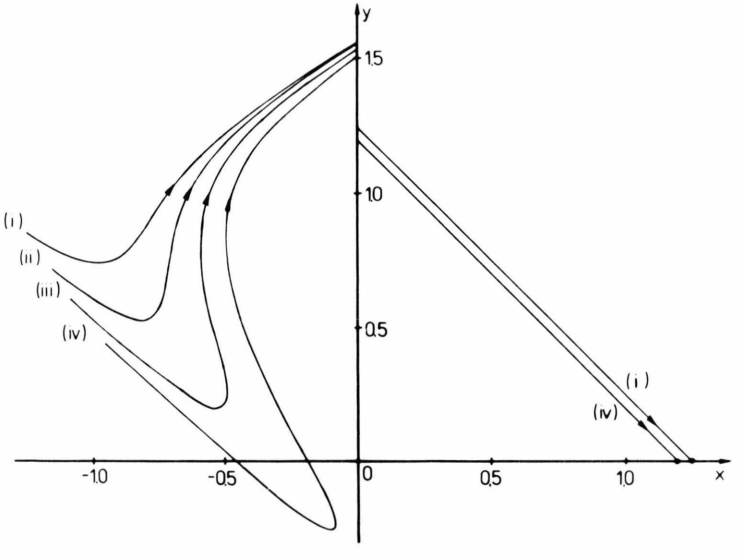

Fig. 7. Pieces of the stable manifold of the right nonperiodic solution (2.21) on the cross section $\Sigma(0)$ according to (2.22), (2.23) for different values of α. Parameter set: $\beta=1$, $\omega=2$, $r=0.8$. (i) $\alpha=0.9$, (ii) $\alpha=0.6$, (iii) $\alpha=0.3$, (iv) $\alpha=0$.

where

$$c_1^{\pm} = \tfrac{1}{2}\left[(x_0^{\pm} + y_0^{\pm} \mp 1)\exp(-t_0) + \beta(t_0 - \ln(2\cosh t_0))\right],$$

$$c_2^{\pm} = \tfrac{1}{2}\left[(x_0^{\pm} - y_0^{\pm} \mp 1)\exp(t_0) - \beta(t_0 + \ln(2\cosh t_0))\right].$$

The special solutions

$$\tilde{x}_{\pm} = \pm 1 - \beta(t \cdot \sinh(t) - \cosh(t)\ln(2\cosh(t)))\,.$$

$$\tilde{y}_{\pm} = -\beta(t \cdot \cosh(t) - \sinh(t)\ln(2\cosh(t))) \qquad (2.17)$$

represent orbits of saddle type. For $\beta = 0$ these solutions reduce to the saddle fixed points of the unforced system. Also, if $t \to \pm\infty$, they are going to $(x, y) = (\pm 1, 0)$. In this case we define orbits of saddle type as solutions which have stable and unstable manifolds of dimension two in the extended phase space [25]. Note that orbits of saddle type must neither be stationary nor periodic.

At $t = 0$, when the forcing has its maximum, the deviation from the fixed points of the unforced system reaches its largest value, i.e.

$$\tilde{x}_{\pm}(0) = \pm 1 + \beta \ln 2, \quad \tilde{y}_{\pm}(0) = 0\,.$$

The stable and unstable manifolds of (2.17) can be calculated by means of the general solutions (2.16). Especially the course of the stable manifold is of interest because it represents the boundary between toppling and rocking.

For the first piece of the stable manifold which belongs to $(\tilde{x}_+, \tilde{y}_+)$ one obtains on the cross section $\Sigma(0)$

$$y_+^s = -x_+^s + 1 + \beta \ln 2\,. \qquad (2.18)$$

Its continuation in the left half plane is given in a parametric form by

$$x_+^s + y_+^s = \beta \ln 2 - 1 + (1 + 1/r)\, e^{-\tau} - \beta(1 - 1/r)\ln(1 + e^{-2\tau}).$$

$$x_+^s - y_+^s = \beta \ln 2 - 1 + (1 - 1/r)\, e^{\tau} - \beta \ln(1 + e^{2\tau}) - \beta e^{2\tau} \ln(1 - e^{2\tau})/r\,. \qquad (2.19)$$

Similar expressions are valid for the unstable manifold. The course of the stable manifold is shown in Fig. 6 for different r values. In the left (or right) half plane there is at most one crossing of manifolds, i.e. the shown pieces of the stable manifold are going to infinity without further windings. Initial conditions above the stable manifold in Fig. 6 result in toppling the block.

The second example of a transient forcing is given by the equation of motion

$$\dot{x} = y, \quad \dot{y} = x \mp 1 - \beta \exp(-\delta t)\cos(\omega t) \quad (\delta > 0) \qquad (2.20)$$

with the usual impact rule (1.2) and sign convention. The same forcing was considered by Varghese and Thorp [7, 8] in transiently driven pendulum systems. Also in this example our primary aim is to describe analytically some pieces of the boundary of the domain of attraction of the stable equilibrium which is located at the origin. The transiently driven system (2.20) has special orbits of saddle type given by

$$\tilde{x}_{\pm} = \pm 1 + \frac{\beta \exp(-\delta t)}{(1 + \omega^2 + \delta^2)^2 - 4\delta^2}\left[(1 + \omega^2 - \delta^2)\cos(\omega t) + 2\delta\omega \sin(\omega t)\right],$$

$$\tilde{y}_{\pm} = -\frac{\beta \exp(-\delta t)}{(1 + \omega^2 + \delta^2)^2 - 4\delta^2}\left[\delta(1 - \omega^2 - \delta^2)\cos(\omega t) + (1 + \omega^2 + \delta^2)\omega \sin(\omega t)\right] \qquad (2.21)$$

whose manifolds can be calculated in the usual manner. On the cross section $\Sigma(0)$ the first pieces of the stable manifold of the solutions $(\tilde{x}_+, \tilde{y}_+)$ (see (2.21)) are given by

$$y_+^s = -x_+^s + 1 + \frac{\beta(1 + \delta)}{\omega^2 + (1 + \delta)^2} \qquad (2.22)$$

in the right half plane, and the continuation in the left half plane by

$$x_+^s + y_+^s = \Big\{1 + 1/r + 2(1/r - 1)\,\bar{\gamma} \cdot e^{-\delta\tau}\left[(1 + \omega^2 - \delta^2)\cos\omega\tau + 2\delta\omega\sin\omega\tau\right] + \frac{(1 - 1/r)\,\beta\, e^{-\delta\tau}}{\omega^2 + (1 - \delta)^2}\left[(1 - \delta)\cos\omega\tau + \omega\sin\omega\tau\right]\Big\} \cdot e^{-\tau} - 1 + \frac{\beta(1 + \delta)}{\omega^2 + (1 + \delta)^2}\,,$$

$$x_+^s - y_+^s = \Big\{1 - 1/r - 2\bar{\gamma} \cdot e^{-\delta\tau}\left[(1 + \omega^2 - \delta^2)\cos\omega\tau + 2\delta\omega\sin\omega\tau\right]/r - \frac{(1 - 1/r)\,\beta\, e^{-\delta\tau}}{\omega^2 + (1 - \delta)^2}\left[(1 - \delta)\cos\omega\tau + \omega\sin\omega\tau\right]\Big\} \cdot e^{\tau} - 1 + \frac{\beta(1 - \delta)}{\omega^2 + (1 - \delta)^2}\,, \qquad (2.23)$$

where

$$\bar{\gamma} = \frac{\beta}{[\omega^2 + (1 - \delta)^2]\,[\omega^2 + (1 + \delta)^2]}\,.$$

For $\delta = 0$ we obtain the expressions which describe periodic forcing (2.11). Similar expressions can be

given for the first pieces of the stable manifold of the solution $(\tilde{x}_-, \tilde{y}_-)$. The pieces of the stable manifold given by (2.22) and (2.23) for different α are represented in Figure 7. However, only the first bend of the winding manifolds is shown. In the case of transiently forced systems on a given cross section $\Sigma(t_0)$ there may exist only a finite number of crossings with the straight lines representing the heteroclinic solutions of the unforced and undamped system [8]. Because of the wrinkling stable manifold the basin boundary for the stable fixed point (0, 0) may be very complicated but actually it is not a fractal. Varghese and Thorp [8] denote such boundaries truncated fractals.

3. Melnikov Analysis of the Nonlinear Problem

In this section for small excitation and energy loss the Melnikov method is applied to prove the existence of Smale horseshoes in the dynamics of the rocking block. The prerequisite to the application of this method is that the equations of motion can be written as the sum of an autonomous system with homoclinic (heteroclinic) orbits and a small time-periodic perturbation. Introducing of a small parameter $\beta \equiv \varepsilon\tilde{\beta}$ $(0 \leq \varepsilon \ll 1)$, (1.1) can be written as

$$\dot{x} = y,$$
$$\dot{y} = \mp\frac{1}{\alpha}\sin[\alpha(1 \mp x)] - \varepsilon\tilde{\beta}\cos[\alpha(1 \mp x)]\cos(\omega t), \quad (3.1)$$

where the upper (lower) sign indicates the right (left) half plane of the phase space. To include the damping at impact, we assume that the coefficient of restitution r is near 1 and define a new coefficient $\tilde{r}$ by

$$(1 - r^2) \equiv \varepsilon\tilde{r}, \quad (3.2)$$

where ε is the small parameter and $\tilde{r}$ is $O(\varepsilon^0) = O(1)$. The usual Melnikov method is developed for sufficiently differentiable systems $(C^r, r \geq 2)$. In the appendix we show that this method can be extended to piecewise smooth systems like (3.1). The corresponding unperturbed system $(\varepsilon = 0)$

$$\dot{x}_0 = y_0, \quad \dot{y}_0 = \mp\frac{1}{\alpha}\sin[\alpha(1 \mp x_0)] \quad (3.3)$$

has the energy as a first integral

$$H = \tfrac{1}{2}(y_0)^2 + \frac{1}{\alpha^2}\cos[\alpha(1 \mp x_0)], \quad (3.4)$$

and the unperturbed solution set contains a heteroclinic orbit which connects the saddle points at $(x_0, y_0) = (\pm 1, 0)$. The Poincaré map of the perturbed system (3.1) for sufficiently small ε has unique hyperbolic saddle points near the unperturbed ones [9]. The heteroclinic Melnikov function, which is a first order measure of the distance between stable and unstable manifolds of hyperbolic fixed points in the Poincaré map, may be written in the form (see appendix)

$$M(t_0) = M_D + M_S, \quad M_S(t_0) = \int_{-\infty}^{\infty} \hat{X}H \, dt, \quad (3.5)$$

where $\hat{X}$ is the perturbation operator

$$\hat{X} = \tilde{\beta}\cos[\alpha(1 \mp x_0)]\cos(\omega t)\frac{\partial}{\partial y_0}. \quad (3.6)$$

For the explicit calculation of the improper integral in (3.5) the unperturbed heteroclinic orbit $x_0(t, t_0)$ as a function of t and the initial time t_0 must be used. In the case of our system it is appropriate to substitute the space variable x_0 for the integration variable t in (3.5). Taking the discontinuity at $x_0 = 0$ into account, one obtains

$$M_S(t_0) = \tilde{\beta}\int_{-1}^{0}\cos[\alpha(1 + x_0)]\cos[\omega t^-(x_0, t_0)]\,dx_0 + \tilde{\beta}\int_{0}^{1}\cos[\alpha(1 - x_0)]\cos[\omega t^+(x_0, t_0)]\,dx_0, \quad (3.7)$$

where t^- (t^+) is the time function depending upon the initial time t_0 and the space variable x_0 in the phase space region $x_0 < 0$ $(x_0 > 0)$. These functions can be obtained from the unperturbed heteroclinic orbit, which is one of the pendulum type solutions. The two functions t^-, t^+ must be fitted at $x_0 = 0$ so that the whole time function runs continuously at the discontinuity $x_0 = 0$. The short calculation is easy to perform and yields

$$t^-(x_0, t_0) = t_0 - \ln\left[\frac{\tan(\alpha/4)}{\tan(\alpha(1 + x_0)/4)}\right],$$
$$t^+(x_0, t_0) = t_0 + \ln\left[\frac{\tan(\alpha/4)}{\tan(\alpha(1 - x_0)/4)}\right].$$

Insertion of these functions into (3.7) and the substitution $z = 1 - x_0$ yield after some elementary manipulations

$$M_S(t_0) = \tilde{\beta}J(\alpha, \omega)\cos(\omega t_0), \quad (3.8)$$

where

$$J(\alpha, \omega) \equiv 2\int_0^1 \cos(\alpha z)\cos\left(\omega \ln\left[\frac{\tan(\alpha/4)}{\tan(\alpha z/4)}\right]\right)dz. \quad (3.9)$$

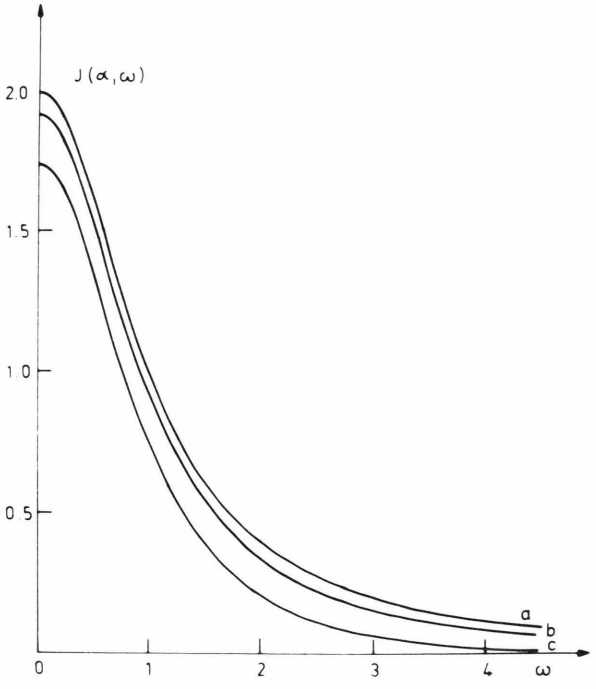

Fig. 8. Representation of the function $J(\alpha, \omega)$.
a) $\alpha=0$, b) $\alpha=0.5$, c) $\alpha=0.9$.

Figure 8 shows the functional dependence of $J(\alpha, \omega)$ for selected values of the block angle α. It should be emphasized that the calculation of (3.8) is based on the upper separatrix of the unperturbed system. Because of the invariance of the equations of motion (3.1) with respect to the transformation

$$x \to -x, \quad y \to -y, \quad \tilde{\beta} \to -\tilde{\beta}$$

one obtains for the lower separatrix the same formula as (3.8) but with a negative sign.

The second part M_D of the Melnikov function is determined by the energy loss owing to the damping at $x_0=0$. It can be calculated by using (1.2), (3.4) and the numerical value of the unperturbed separatrix energy. One finds

$$\Delta E_D = H(y_0(t_A)) - H(y_0(t_B)) = -\frac{2(1-r^2)}{\alpha^2} \sin^2(\alpha/2),$$

and moreover, with (3.2)

$$\Delta E_D = -\varepsilon \frac{2\tilde{r}}{\alpha^2} \sin^2(\alpha/2) = \varepsilon M_D .$$

The condition for heteroclinic bifurcation arises from the fact that the Melnikov function $M(t_0)=M_D+M_S$ must have quadratic zeros as a function of t_0. One finds the condition

$$\tilde{\beta} = \frac{2\tilde{r} \sin^2(\alpha/2)}{\alpha^2 J(\alpha, \omega)}, \tag{3.10}$$

where $J(\alpha, \omega)$ is the function defined by (3.9). For larger values of the excitation $\tilde{\beta}$ than in (3.10) we find transverse intersections of stable and unstable manifolds of the hyperbolic fixed points of the associated Poincaré map. Note that (3.10) is restricted to small excitation and damping. The block parameter α is arbitrary. On the other hand, the bifurcation condition for the slender block case (2.14) is valid for all values of β and r.

The integral in (3.9) can be calculated by elementary methods in the limiting case of slender block motion, i.e. for $\alpha \ll 1$. The result is

$$J(\alpha \to 0, \omega) = 2/(1+\omega^2),$$

and therefore the bifurcation condition (3.10) becomes

$$\tilde{\beta} = \tilde{r}(1+\omega^2)/4 \tag{3.11}$$

in this limit. This result is in a complete correspondence with the result of Sect. 2, especially with (2.14). Using $\beta=\varepsilon\tilde{\beta}$ and (3.2) in (2.14), one finds (3.11) up to the first order in the small parameter ε.

4. Summary

We have demonstrated the existence of chaotic orbits in the dynamics of the harmonically forced rocking block by proving the existence of transverse heteroclinic points in the Poincaré map. For the slender block (Sect. 2) an analytical treatment is possible so that the bifurcation condition for the heteroclinic bifurcations is valid for all values of the parameters, i.e. damping, amplitude and frequency. This is important because in many other examples these conditions can be computed only to first order in the size of the perturbation [9, 26–28]. Also the case of block dynamics with a finite block angle α is of this type. Using the Melnikov method, we have obtained, for small excitation and damping, a condition for the heteroclinic bifurcations of the nonlinear problem. The basic integral (3.9) is calculated numerically by a standard procedure, and the result in Fig. 8 shows that there are only small deviations from the slender block case $\alpha \ll 0$ in the range $0<\alpha<1$. Moreover, in the limiting case of slender block motion with small excitation and damping the conditions (2.14) and (3.10) are identical.

The existence of chaotic orbits in the dynamics of the rocking block implies that long range state predictions are impossible. Moreover, the effect of the fractal basin boundaries [6, 29] reduces predictability of the final states of the block. The boundary in phase space which separates rocking from tumbling is determined by the stable manifold of the hyperbolic fixed points. For the slender block we have given an analytical formula for the first pieces of the stable manifold. This is an advantage of the piecewise linear system because in other systems the manifolds can be obtained by numerical methods only.

Transiently driven systems are more appropriate to describe real earthquake dynamics. For man-made structures like towers or nuclear reactors it is important to know the boundary of stability with regard to different families of transient forcings. The boundary in phase space is given by the stable manifolds of special saddle-type solutions. In the examples discussed the analytical calculations of these manifolds can, in principle, be continued to arbitrary length.

Piecewise linear systems like (2.1) are suitable for the analytical calculation of further results characterizing the chaotic dynamics. The unstable manifolds of the periodic solutions (2.3) represent the skeleton of the horseshoe repeller and also of the numerical detected chaotic attractor in the case of large forcing [4]. Also the set of periodic saddle orbits characterizes the properties of the chaotic repeller and attractor, respectively [30–32]. Because the pieces of the considered unstable manifolds can be represented in an analytical form and numerous saddle orbits can be precisely located and even their eigenvalues can be calculated, it should be possible to obtain analytical approximations for further properties (generalized dimensions and thermodynamic functions) which characterize repellers and attractors (see e.g. [33]).

Appendix

We consider the following perturbed Hamiltonian system with a discontinuity at $x=0$:

$$\dot{x}=\frac{\partial H^{+/-}}{\partial y}, \quad \dot{y}=-\frac{\partial H^{+/-}}{\partial y}+\varepsilon f^{+/-}(x, y, t), \tag{A.1}$$

where H^+, f^+ and H^-, f^- are defined for $x>0$ and $x<0$, respectively. The perturbation functions $f^{+/-}$ are periodic in time with period T. At $x=0$ there is an impact rule $y(t_A)=r\,y(t_B)$, where $0\leq r\leq 1$. Regarding the unperturbed system ($\varepsilon=0$, $r=1$) the following assumptions should be fulfilled:

a) There is a saddle point in each half plane and a heteroclinic orbit which connects these points.

b) $\lim\limits_{x\to+0} H^+ = \lim\limits_{x\to-0} H^-$ and $\lim\limits_{x\to+0} f^+ = \lim\limits_{x\to-0} f^-$.

Therefore a continuous Hamiltonian and a continuous perturbation function may be defined in the whole phase plane by

$$H(x, y)\equiv\begin{cases} H^+(x, y) & \text{if } x>0, \\ H^-(x, y) & \text{if } x<0, \\ \lim\limits_{x\to+0} H^+ & \text{if } x=0, \end{cases} \tag{A.2}$$

$$f(x, y, t)\equiv\begin{cases} f^+(x, y, t) & \text{if } x>0, \\ f^-(x, y, t) & \text{if } x<0, \\ \lim\limits_{x\to+0} f^+ & \text{if } x=0, \end{cases} \tag{A.3}$$

We next take the cross section $\Sigma(t_0)=\{(x, y, t)\,|\,t=t_0, t_0+T, \ldots\}$ and consider the Poincaré map $P\colon \Sigma\to\Sigma$ induced by the solutions of (A.1). P has unique hyperbolic saddle points near the unperturbed ones for all sufficiently small ε [9]. The discontinuity should not be located in the ε neighbourhood of the fixed points. To find a measure of the distance between the perturbed manifolds up to the first order in ε, we use the possibility that phase space distances can be measured in units of the energy. The energy value of the unperturbed separatrix is used as the reference energy. It is well known that a fixed point displacement of order ε yields an energy shift of order ε^2 only. Therefore the energy of the perturbed fixed points is equal to that of the unperturbed ones to order ε.

Figure 9 shows the qualitative structure of the fixed point manifolds and the corresponding energy values. There is an energy difference between the perturbed manifolds W^S and W^U at a given value of x. To determine this difference at $x=+0$ (or $x=-0$) up to $O(\varepsilon)$ we calculate the energy increments along the unperturbed manifolds. One finds for the unstable manifold [26]

$$\Delta E_U=\varepsilon\int_{-\infty}^{\tau}\hat{X}^- H^-(x_0, y_0)\,\mathrm{d}t$$

and for the stable manifold

$$\Delta E_S=\varepsilon\int_{\tau}^{\infty}\hat{X}^+ H^+(x_0, y_0)\,\mathrm{d}t\,. \tag{A.4}$$

$\hat{X}^{+/-}=f^{+/-}(x_0, y_0, t)\,\partial/\partial y_0$ are the perturbation operators defined for $x>0$ and $x<0$, respectively.

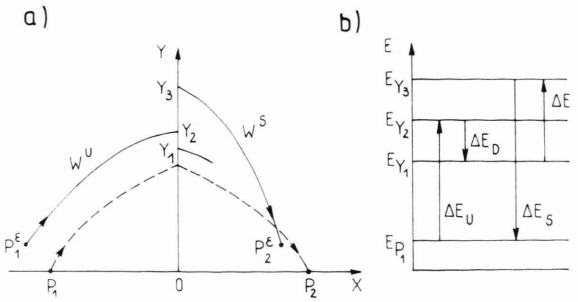

Fig. 9. a) Fixed points and parts of their manifolds for the perturbed (solid curve) and the unperturbed (dashed curve) system. b) Schematic diagram with the energy of the points denoted in a) and the corresponding energy increments.

$(x_0 = x_0(t-t_0),\ y_0 = y_0(t-t_0))$ denotes the unperturbed heteroclinic solution and τ is the value of the time parameter at the discontinuity. Therefore, taking into account the energy loss due to impact ΔE_D, the distance between the stable and unstable manifolds in energy units at $x = +0$ is given by

$$\Delta E = \Delta E_D + \Delta E_S + \Delta E_U = \Delta E_D + \varepsilon \int_{-\infty}^{\infty} \hat{X} H(x_0, y_0)\, dt, \tag{A.5}$$

Note that this distance depends on the chosen cross section $\Sigma(t_0)$. In (A.5) we have introduced the perturbation operator $\hat{X} = f(x_0, y_0, t)\,\partial/\partial y_0$ and the Hamiltonian H (see (A.2) and (A.3)) which are defined in the whole phase plane. It must be underlined that the integrand $\hat{X}H(x_0, y_0)$ in (A.5) is not smooth at $t = \tau$ but nevertheless the integral is well defined. Assuming that the energy loss due to impact is small, i.e. $\Delta E_D = \varepsilon M_D$ with $M_D = O(1)$ (see Sect. 3) the Melnikov function can be defined as usual:

$$\Delta E(t_0) = \varepsilon M(t_0)$$

with a dissipative and an oscillating part,

$$M(t_0) = M_D + M_S(t_0), \tag{A.6}$$

where according to (A.5)

$$M_S(t_0) = \int_{-\infty}^{\infty} \hat{X} H(x_0, y_0)\, dt\,.$$

If this function $M(t_0)$ has simple zeros, then there exist transverse intersections of the regarded stable and unstable manifolds.

[1] M. Aslam, W. G. Godden, and D. T. Scalise, J. Struct. Div. ASCE **106,** 377 (1980).
[2] C. S. Yim, A. K. Chopra, and J. Penzien, J. Earthquake Engng. Struct. Dyn. **8,** 565 (1980).
[3] P. D. Spanos and A. S. Koh, J. Eng. Mech. Div. Amer. Soc. Civ. Engrs. **110,** 1627 (1984).
[4] J. Hogan, Proc. Roy. Soc. London **A 425,** 441 (1989).
[5] W. K. Tso and C. M. Wong, Earthquake Engng. Struct. Dyn. **18,** 89 (1989).
[6] C. Grebogi, E. Ott, and J. A. Yorke, Physica **24D,** 243 (1987).
[7] M. Varghese and J. S. Thorp, Phys. Rev. Lett. **60,** 665 (1988).
[8] M. Varghese and J. S. Thorp, IEEE Trans. Circ. Syst. **35,** 825 (1988).
[9] J. Guckenheimer and P. J. Holmes, Nonlinear Oscillations, Dynamical Systems and Bifurcations of Vector Fields, Springer, New York 1983.
[10] S. W. Shaw and P. J. Holmes, Phys. Rev. Lett. **51,** 623 (1983).
[11] S. W. Shaw and P. J. Holmes, J. Sound Vibrations **90,** 129 (1983).
[12] S. W. Shaw, J. Appl. Mech. **52,** 453 (1985).
[13] M. B. Hindmarsh and D. J. Jeffries, J. Phys. **A 17,** 1791 (1984).
[14] T. Kiemel and P. J. Holmes, IMA J. Math. Appl. Med. Biol. **4,** 145 (1987).
[15] S. N. Chow and S. W. Shaw, J. Diff. Equat. **65,** 304 (1986).
[16] J. N. Schulman, Phys. Rev. **A 28,** 477 (1983).
[17] J. M. T. Thompson and R. Ghaffari, Phys. Rev. **A 27,** 1741 (1983).
[18] H. M. Isomäki, J. Von Boehm, and R. Räty, Phys. Lett. **107 A,** 343 (1985).
[19] H. M. Isomäki, J. Von Boehm, and R.Räty, Phys. Lett. **126 A,** 484 (1988).
[20] N. K. Gavrilov and L. P. Shilnikov, Mat. Sbornik **88,** 467 (1972).
[21] N. K. Gavrilov and L. P. Shilnikov, Mat. Sbornik **90,** 139 (1973).
[22] P. J. Holmes, Lecture Notes in Mathematics **898,** 164 (1981).
[23] A. L. Bertozzi, SIAM J. Math. Anal. **19,** 1271 (1988).
[24] M. Taki, Phys. Rev. **B 35,** 3267 (1987).
[25] S. Wiggins, Introduction to Applied Nonlinear Dynamical Systems and Chaos, Springer, New York 1990, p. 607.
[26] B. Bruhn, Phys. Scripta **35,** 7 (1987).
[27] B. P. Koch and R. W. Leven, Physica **16D,** 1 (1985).
[28] B. P. Koch and B. Bruhn, Z. Naturforsch. **44a,** 1155 (1989).
[29] F. C. Moon and G. X. Li, Phys. Rev. Lett. **55,** 1439 (1985).
[30] D. Auerbach, P. Cvitanovic, J. P. Eckmann, G. H. Gunaratne, and I. Procaccia, Phys. Rev. Lett. **58,** 2387 (1987).
[31] G. H. Gunaratne and I. Procaccia, Phys. Rev. Lett. **59,** 1377 (1987).
[32] D. Auerbach, B. O'Shaughnessy, and I. Procaccia, Phys. Rev. A **37,** 2234 (1988).
[33] T. Tel, Transient Chaos, in: Directions in Chaos, Vol. 3 (Hao Bai-lin, ed.), World Scientific Publ. Co., Singapore 1990.